RESEARCH ARTICLE

Disease Models & Mechanisms 6, 206-216 (2013) doi:10.1242/dmm.010108

A yeast model for amyloid-β aggregation exemplifies the role of membrane trafficking and PICALM in cytotoxicity

Fabien D'Angelo[1,*], Hélène Vignaud[1,*], Julie Di Martino[1], Bénédicte Salin[1], Anne Devin[1], Christophe Cullin[1,‡] and Christelle Marchal[1]

SUMMARY

Alzheimer's disease is the most common neurodegenerative disease, associated with aggregation of amyloid-β (Aβ) peptides. The exact mechanism of neuronal cell dysfunction in Alzheimer's disease is poorly understood and numerous models have been used to decipher the mechanisms leading to cellular death. Yeast cells might be a good model to understand the intracellular toxicity triggered by Aβ peptides. Indeed, yeast has been used as a model to examine protein functions or cellular pathways that mediate the secretion, aggregation and subsequent toxicity of proteins associated with human neurodegenerative disorders. In the present study, we use the yeast *Saccharomyces cerevisiae* as a model system to study the effects of intracellular Aβ in fusion with green fluorescent protein. We sent this fusion protein into the secretory pathway and showed that intracellular traffic pathways are necessary for the generation of toxic species. Yeast PICALM orthologs are involved in cellular toxicity, indicating conservation of the mechanisms of toxicity from mammals to yeast. Finally, our model demonstrates the capacity for intracellular Aβ to cross intracellular membranes and target mitochondrial organelles.

INTRODUCTION

Alzheimer's disease (AD) was first described 100 years ago and is a progressive neurodegenerative pathology leading to gradual cognitive and behavioral changes and loss of memory (Selkoe and Podlisny, 2002). It is associated with the presence of region-specific amyloid-β (Aβ) deposits in the brain. These amyloid plaques form one of the neuropathological hallmarks of AD. The *APP* gene encodes the amyloid precursor protein (APP), which encompasses the Aβ peptides. Differential cleavage of APP produces amyloid peptides of 40 ($A\beta_{40}$) or 42 ($A\beta_{42}$) amino acids in length; the $A\beta_{40}$ species are considered to be less toxic. Although Aβ aggregation is correlated with the extracellular deposition of terminal amyloid plaques in AD patients and AD mouse models, Aβ species also accumulate within the cell, including inside multivesicular bodies (Almeida et al., 2006; Langui et al., 2004; Takahashi et al., 2002), lysosomes or other vesicular compartments (Nixon, 2007; Shie et al., 2003). Recent publications have confirmed the important role played by intracellular Aβ, whether it is produced through the secretion pathway, by transfection or by uptake from the medium (Echeverria et al., 2004; Hansson Petersen et al., 2008; Hu et al., 2009; Kandimalla et al., 2009; Rebeck et al., 2010).

Different biological model systems including Aβ-transgenic *Caenorhabditis elegans* worm (Link, 1995), *Drosophila melanogaster* flies (Crowther et al., 2005; Iijima et al., 2004) and mammalian cell cultures (Magrané et al., 2004) have been used to study the role of intracellular Aβ. These biological systems have identified general effects such as mitochondrial organization (Zhao et al., 2010; Iijima-Ando et al., 2009) or folding machinery (Fonte et al., 2002; Magrané et al., 2004) as targets or regulators of toxic Aβ species. These findings have been confirmed in vivo (Hoshino et al., 2011) and are similar to the changes found in pathogenic situations. This supports the notion that part of the complex process leading to AD can be reliably studied at the cellular level. However, the different cell models used so far have not revealed any molecular mechanisms that could account for the toxicity of Aβ. In addition, pharmacological approaches based on molecules that interfere with Aβ formation have not been productive. This has raised several questions concerning the paradigm and the models used for these strategies. So far, no simple organism that can be manipulated for a high throughput screening can be used as a 'gold standard' for Aβ toxicity.

Yeast cells are suitable for such screening and have been widely used to pinpoint gene networks and chemical compounds that can modulate amyloid toxicity. This was particularly the case for Parkinson's disease (Willingham et al., 2003; Cooper et al., 2006; Franssens et al., 2010) and amyotrophic lateral sclerosis (Sun et al., 2011; Ju et al., 2011; Fushimi et al., 2011). Although this experimental model has been successfully used to monitor the aggregation pattern of Aβ (Bagriantsev and Liebman, 2006; Caine et al., 2007; von der Haar et al., 2007), these first yeast systems failed to recapitulate the toxic properties of this peptide. In these previous studies, Aβ was expressed in the yeast-cell cytoplasm. Very recently, a new screen based on a secreted form of Aβ in yeast revealed the importance of the endocytic pathway in cellular toxicity (Treusch et al., 2011).

[1]Institut de Biochimie et Génétique Cellulaires, CNRS UMR 5095, Université Bordeaux 2, Victor Segalen, 33077 Bordeaux, France
*These authors contributed equally to this work
‡Author for correspondence (cullin@ibgc.cnrs.fr)

Received 23 April 2012; Accepted 2 August 2012

© 2012. Published by The Company of Biologists Ltd
This is an Open Access article distributed under the terms of the Creative Commons Attribution Non-Commercial Share Alike License (http://creativecommons.org/licenses/by-nc-sa/3.0), which permits unrestricted non-commercial use, distribution and reproduction in any medium provided that the original work is properly cited and all further distributions of the work or adaptation are subject to the same Creative Commons License terms.

TRANSLATIONAL IMPACT

Clinical issue

The amyloid cascade hypothesis proposes a fundamental role for amyloid-β (Aβ) in AD. Although found mainly as extracellular deposits, Aβ seems to impair intracellular mechanisms following the efficient uptake of the peptide. To date, simple cellular systems have not been used to extensively study the toxic mechanisms induced by intracellular Aβ and, in particular, to address the role of Aβ secretion and endocytosis in cellular toxicity. Yeast was previously used as a model to study amyloid infectiosity and toxicity in other neurodegenerative diseases. More recently, *S. cerevisiae* has also been successfully applied to pinpoint genes involve in Aβ toxicity; many findings were later confirmed in other eukaryotic models.

Results

This paper presents a new and versatile model involving yeast expression of Aβ. The authors established a system in which Aβ enters the secretory pathway, goes to the plasma membrane and subsequently becomes toxic to the cells. Aβ toxicity depends on the form of Aβ expressed, with the arctic mutant ($Aβ_{ARC}$) being more toxic than the wild-type ($Aβ_{42}$), and on the presence of proteins involved in protein trafficking pathways, such as PICALM. Notably, the gene encoding PICALM is a known susceptibility factor for AD. Yeast orthologs of mammalian PICALM increase Aβ toxicity in this yeast model (in contrast to previous findings in another yeast model that PICALM limits deleterious effects). The authors also demonstrate that Aβ can cross membranes and target mitochondria.

Implications and future directions

These results indicate that Aβ must be translocated via the secretory pathway to induce toxicity in yeast cells. This finding is in agreement with other yeast Aβ-expression models, but is contradictory with respect to the role of the endocytic pathway, highlighting the importance of tailoring the experimental model used to study Aβ toxicity (which can be influenced by level of expression, stabilization of translational fusion, etc.). This model also pinpoints the mechanisms by which Aβ disrupts cytoplasmic functions and offers a powerful platform for their characterization. Finally, these results support the idea that mechanisms of Aβ toxicity in yeast parallel those in mammalian cells, meaning that yeast-based approaches will continue to offer new insights into AD.

In the present study we demonstrate that targeting Aβ in the secretory pathway produces toxic species. The toxicity depends on the allele expressed, arctic mutants being more harmful than wild-type Aβ. Disturbance of cell-traffic routes (i.e. secretion, endocytosis, recycling or traffic between Golgi and vacuoles) reduced the toxic effects of Aβ. Together, these results indicate that in our yeast model, the cellular toxicity is not due to endocytosis dysfunction but rather implicate another cellular target.

RESULTS

Aβ becomes toxic when expressed with a secretory sequence

It has been clearly established that $Aβ_{40}$ or $Aβ_{42}$ expressed in frame with reporter genes such as GFP (Caine et al., 2007) or the functional domain of Sup35 (von der Haar et al., 2007; Bagriantsev and Liebman, 2006) does not lead to yeast death. We fully reproduced this result because, regardless of whether the wild-type ($Aβ_{42}$) or arctic mutant ($Aβ_{ARC}$) was expressed, the number of colonies formed on galactose (inducing conditions for expression of Aβ-GFP) or on dextrose (repressing conditions) was the same (Fig. 1). In both cases, the pattern of aggregation was similar, with the presence of bright dots. Because Aβ toxicity is observed when this peptide is secreted in the fly model of AD (Finelli et al., 2004; Iijima et al., 2004), it was therefore challenging to test the toxicity to yeast of Aβ species entering the secretion pathway. When GFP was fused to the mating factor α (MFα) prepro-leader sequence secretion signal derived from the precursor of the *Saccharomyces cerevisiae* MFα (Kurjan and Herskowitz, 1982), there was no marked effect on the colony forming unit (CFU) capacity. Previous studies based on four different yeast secretion signal sequences (i.e. *INU1*, *SUC2*, *PHO5* and *MEL1*) did not report any toxicity for secreted GFP (Li et al., 2002). By contrast, we observed that expression of MFα-$Aβ_{42}$-GFP reduced viability (decrease in CFU) and extended the time required to obtain visible colonies (Fig. 1). Both of these effects were exacerbated when $Aβ_{ARC}$ was expressed under the same conditions.

One of the problems with GFP chimeric proteins is that cellular properties such as toxicity could be due to GFP itself. We tested this hypothesis by removing GFP from the plasmids (supplementary material Fig. S1) and observed the same toxic phenotypes. The toxicity was clearly lower, but the arctic mutant was still more deleterious than the wild-type Aβ. Western blot analysis revealed that the level of expression was greatly diminished without GFP (supplementary material Fig. S1). GFP probably helps to stabilize Aβ peptide but it is clear that all of the toxic properties of Aβ-GFP can be attributed to the Aβ part of the chimeric protein.

The MFα-GFP chimer exhibited a low and non-diffuse fluorescence pattern, whereas the MFα-Aβ-GFP proteins could not be detected by fluorescence. This low signal (or even absence of signal) might be due to a low level of expression, improper GFP folding, post-translational modification or a combination of these factors. To test the possibility of GFP misfolding due to Aβ aggregation (Wurth et al., 2002), we engineered additional constructs with a linker sequence inserted between Aβ and GFP. The two new chimeric proteins were as toxic as the two previous constructs (Fig. 1) and could now be detected in yeast cells. This finding ruled out the possibility of GFP misfolding due to its expression throughout the secretory pathway. The same Aβ-GFP chimeric proteins behaved differently in the cytoplasm (formation of foci and nontoxic) and in the secretory pathway (non-ponctiform and toxic). We next checked the processing of MFα-Aβ-GFP proteins.

Processing of MFα-Aβ-GFP

Expression of GFP, $Aβ_{42}$-GFP or $Aβ_{ARC}$-GFP resulted in one species (26 or 31 kDa, respectively) that cross-reacts with anti-GFP antibodies (Fig. 2A, left). By contrast, the secreted forms of $Aβ_{42}$-GFP or $Aβ_{ARC}$-GFP resulted in three bands (Fig. 2A, right). The smallest (about 34 kDa) and largest species (about 50 kDa) were the most abundant. During galactose induction, these two species were detected first (Fig. 2B); the incapacity to detect the intermediate species early on during induction was probably due their low concentration (below the sensitivity threshold). The mobility of the smallest species is consistent with the production of the mature proteins. This process requires Kex2p, an endoprotease in the late Golgi compartment (Redding et al., 1991) that is involved in processing α-factor (Julius et al., 1984). To test this hypothesis, we analyzed the different protein species produced in a *Δkex2* strain (Fig. 3A). Indeed, the smallest species were no longer detected, as expected if they were produced by Kex2p. Among the three bands revealed by anti-GFP antibodies, the

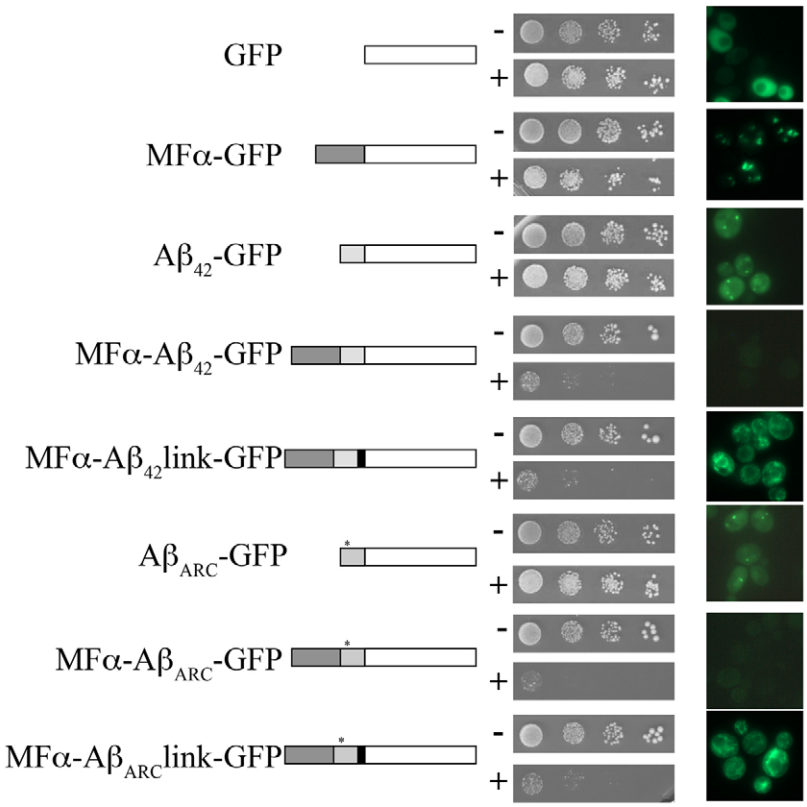

Fig. 1. Aβ aggregation and yeast growth. Each coding sequence is represented by a rectangle: white for GFP, dark gray for secretory signal, gray for Aβ and black for the gly-ala linker. * is used for the $A\beta_{42}$ arctic allele. Left: Tenfold dilutions of exponentially growing cultures of BY4742 cells transformed with plasmids carrying the different chimeric constructions under the GAL10 promoter were spotted onto SD (–) or SG (+) agar supplemented with 20 mg/l histidine, 20 mg/l lysine and 60 mg/l leucine. The cells were incubated at 30°C for 3 days. Right: The cells were also grown for 6 hours in SG liquid medium supplemented with 0.67% casamino acids to induce the expression of the chimeric proteins and were examined by epifluorescence microscopy.

highest weight band was bigger than the MFα-$A\beta_{42}$-GFP species (41 kDa). The prepro-α-factor is glycosylated through the yeast secretory pathway (Julius et al., 1984), and the higher mobility could be due to glycosylation of prepro-Aβ-GFP species. To test this hypothesis, we added a deglycosylation mix to the crude extract. After enzyme treatment, the proteins were analyzed by western blot (Fig. 3B). The highest mobility band was no longer detected whereas the intermediate band was more intense, as expected if this band corresponds to the unglycosylated form of prepro-Aβ-GFP. The ratio of these three bands depended on the preparation method of the crude extracts (data not shown). This might have been due to a particular protection against proteases and we thus tested the sensitivity of these proteins to proteases. The extracts prepared from yeast spheroplasts revealed four bands instead of three. Proteinase K analysis of the P13 fraction (corresponding to the 13,000 ***g*** pellet fraction of yeast lysate prepared under mild conditions) identified the lowest-mobility band as PK-resistant entities (Fig. 3C). This finding is consistent with an intra-membranous localization of glycosylated prepro-Aβ-GFP, but indicates that most of the mature form (Aβ-GFP) is sensitive to the protease (i.e. is not imbedded in the membranous compartment). Because the proteins enter the secretory pathway, we searched for the presence of GFP species in the medium. It has been previously reported that GFP expressed in frame with different secretory signal peptides did enter the secretory pathway but was not detected in the medium (Li et al., 2002). With our constructs based on the prepro-α-factor peptide, we did not detect any GFP species in the medium using either fluorescence or western blot of concentrated medium (data not shown).

Disturbance of cell-traffic pathways decreases the toxicity triggered by Aβ chimeric proteins

Prepro-Aβ-GFP enters the secretory pathway and is clearly toxic to yeast cells. Moreover, the *PICALM* gene, which encodes phosphatidylinositol-binding clathrin assembly protein in mammals, has been recently described as a new susceptibility gene for AD (Harold et al., 2009). In mammalian cells, the neuron-specific AP180 protein and its ubiquitously expressed homolog PICALM (also known as CALM, clathrin assembly lymphoid myeloid leukemia protein) are adaptor proteins that participate in clathrin-mediated endocytosis. Adaptors determine the trafficking itinerary of cargos and their steady-state distributions within the cell (Fig. 4). The yeast AP180 proteins are yeast homologs of PICALM (Wendland and Emr, 1998). They share 48% identity, and 25.5% (Yap1801) and 26.5% (Yap1802) identity with PICALM protein. Deletion of *YAP1801* and *YAP1802* clearly decreased the toxicity induced by MFα-$A\beta_{42}$-GFP and MFα-$A\beta_{ARC}$-GFP by lowering the growth inhibition (Table 1; supplementary material Fig. S2). We investigated whether the mammalian gene encoding PICALM could complement the *yap1801* and *yap1802* mutants. PICALM has two splice variants designated long (L) and short (S) according to the number of amino acids. The two mouse cDNAs were subcloned into a multi-copy galactose-induced plasmid. The L isoform on its own was toxic in yeast (data not shown) and could thus not be used. Expression of the S isoform of PICALM in *yap1801-yap1802* double-deleted yeast mutants partially restored the growth inhibition observed when MFα-$A\beta_{42}$-GFP or MFα-$A\beta_{ARC}$-GFP were expressed in wild-type cells (Fig. 5). This suggests that mouse PICALM protein is able to complement YAP loss of

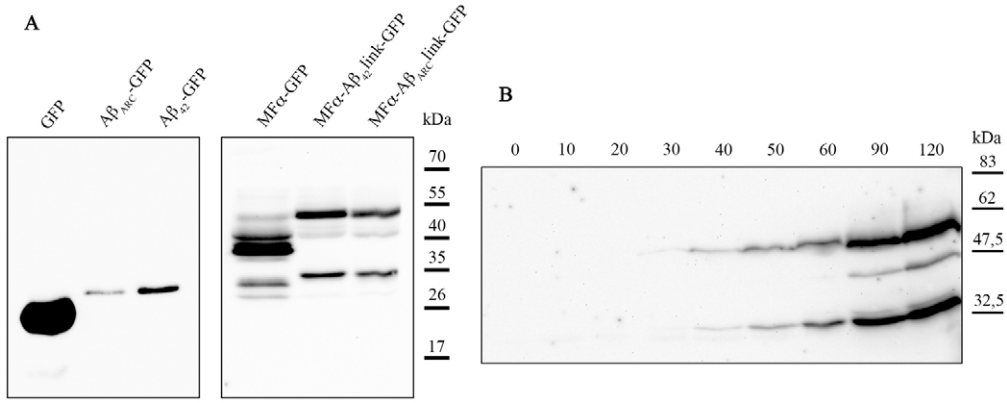

Fig. 2. Maturation of secreted forms of Aβ. (A) BY4742 cells expressing the different chimeric proteins (6 hours of expression) were collected for total-protein extraction. Equal quantities of proteins were separated by SDS-PAGE on a 12% polyacrylamide gel and were then transferred onto a nitrocellulose membrane and exposed to monoclonal anti-GFP antibodies as indicated. (B) At different time points of the induction (shown in minutes), cells were collected for total-protein extraction. Equal quantities of proteins were separated by SDS-PAGE on a 12% polyacrylamide gel and were then transferred onto a nitrocellulose membrane and exposed to monoclonal anti-GFP antibodies.

function and that mammal and yeast proteins share a crucial role in Aβ toxicity.

In mammalian cells, PICALM interacts with the clathrin-associated adaptor protein complex-2 (AP-2) (Owen et al., 2000), and depletion of PICALM triggers delocalization of the AP-1 adaptor complex (Meyerholz et al., 2005). The toxicity induced by MFα-$Aβ_{42}$-GFP and MFα-$Aβ_{ARC}$-GFP was partially suppressed when different subunits of the AP-1 and AP-2 complex were deleted. Two other classes of adaptors participate with AP-1 in clathrin-mediated transport between the trans-Golgi network (TGN) and endosomes (Fig. 4): Gga2p protein and epsin-like protein Ent5p (Costaguta et al., 2006). The absence of these two proteins also restored growth (Table 1). The only identified cargo that is internalized by Yap1801 and Yap1802 is the vSNARE Snc1p (Burston et al., 2009). Snc1p recycles to the plasma membrane and this recycling requires Rcy1p (Galan et al., 2001). We observed

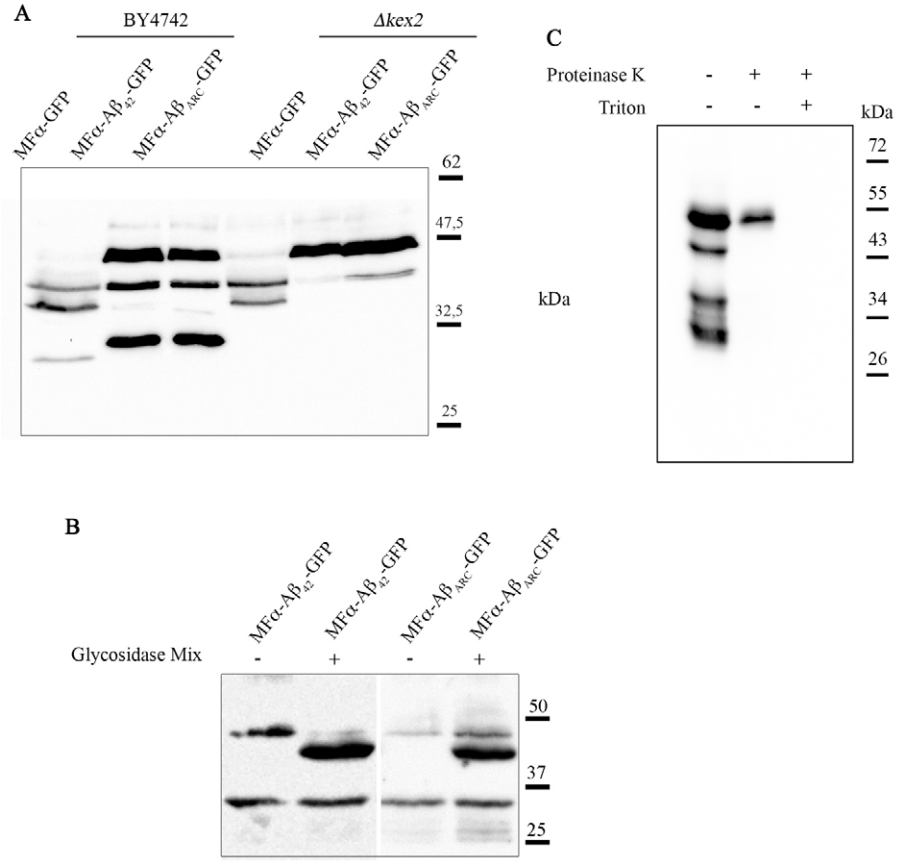

Fig. 3. The secreted forms are glycosylated and processed by Kex2p. (A) BY4742 wild-type or *Δkex2* cells expressing the different chimeric proteins (6 hours of expression) were collected for total-protein extraction. Equal quantities of proteins were separated by SDS-PAGE on a 12% polyacrylamide gel, transferred onto a nitrocellulose membrane and then exposed to monoclonal anti-GFP antibodies. (B) BY4742 expressing the different chimeric proteins (6 hours of expression) were collected for total-protein extraction and submitted or not to a deglycosylation enzyme mix. Equal quantities of proteins were separated by SDS-PAGE on a 12% polyacrylamide gel, transferred onto a nitrocellulose membrane and exposed to monoclonal anti-GFP antibodies. (C) After spheroplast fractionation of BY4742 cells expressing MFα-$Aβ_{ARC}$-GFP, P13 fractions were treated with proteinase K (0.3125 mg/ml) in the presence (+) or absence (–) of 5% Triton X-100, resolved by SDS-PAGE and then analyzed by immunoblotting.

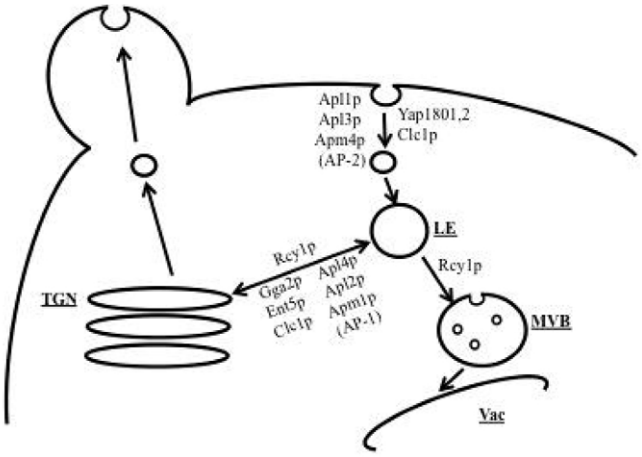

Fig. 4. Schematic view of endocytosis and recycling in yeast. Cellular compartments are indicated: late endosome (LE), multivesicular body (MVB) shown with intralumenal vesicles, vacuole (Vac), and trans-Golgi network (TGN). The proteins involved in some of the steps of endocytosis and recycling are indicated next to the arrows (note that not all proteins are included, only those tested in this study).

Table 1. Growth capacity of different strains expressing MFα-Aβ$_{42}$-GFP or MFα-Aβ$_{arc}$-GFP

Complex	Strain	Viability restoration
AP1	*Δapl4*	++
	Δapl2	+
	Δapm1	++
AP1-associated	*Δgga2*	+
	Δent5	+
	Δclc1	+
	Δrcy1	+++
AP2	*Δapl3*	++
	Δapl1	++
	Δapm4	++
AP2-associated	*Δyap1801*	++
	Δyap1802	++
	Δyap1801/Δyap1802	++

The growth capacity was evaluated by spotting assays and was compared to wild-type strains expressing the same chimeric proteins or carrying an empty vector.

that the toxicity induced by MFα-Aβ$_{42}$-GFP and MFα-Aβ$_{ARC}$-GFP was strongly suppressed when *RCY1* was deleted (Table 1; supplementary material Fig. S2). Our findings indicate that defects in the endocytic or recycling pathway reduce the toxicity triggered by the Aβ-GFP chimeric proteins. It is also clear that MFα-Aβ$_{42}$-GFP and MFα-Aβ$_{ARC}$-GFP are still toxic in such background.

Cellular localization of Aβ-GFP

After induction of MFα-Aβ$_{42}$-GFP and MFα-Aβ$_{ARC}$-GFP in wild-type cells, proteins present a dual pattern of punctuate and filamentous fluorescent structures (Fig. 1). These two patterns are not found systematically because filamentous organization is observed in most of the fluorescent cells whereas punctuate foci are only present in some of them. In mutants that are lower in Aβ toxicity and defective for traffic pathways, the ratio of the two fluorescence patterns is inversed. Most of the cells present small foci and we occasionally observed the filamentous pattern (Fig. 6). This correlates the presence of filamentous aggregates with Aβ toxicity and suggests that the punctuate structures correspond to membrane vesicles.

In mutant strains defective in the early stages of endocytosis, such as the *Δsnf7* mutant, part of GFP fluorescence is associated with the plasma membrane (Fig. 6). In such mutants, membrane invagination into multi-vesicular bodies (MVB) is impaired (Babst et al., 2002) and this decreases the rate of endocytosis. This result shows that the chimeric proteins are able to reach the plasma membrane. Because none of chimeric proteins were detected in the extracellular medium, we speculate that the proteins could be internalized once they had reached the plasma membrane.

The use of yeast cells expressing red fluorescent protein (RFP) fused to proteins whose localization has been characterized previously (Huh et al., 2003) identified the ER as the sole compartment clearly labeled by Aβ-GFP species (supplementary material Fig. S3). This finding does not rule out the localization of Aβ-GFP on other membrane compartments because the speed of the vesicles makes it unlikely to detect both fluorescent signals when they are not observed simultaneously.

These findings show that disturbances of the endocytic or recycling pathways modify the aggregation pattern of MFα-Aβ$_{42}$-GFP and MFα-Aβ$_{ARC}$-GFP as well as their cellular toxicity.

Hsp104p plays a role in Aβ chimeric protein toxicity

Hsp104p is crucial for the toxicity and aggregation of the polyglutamine Huntingtin protein in yeast (Meriin et al., 2002). Because Hsp104p plays a pivotal role in aggregate formation in yeast, we tested whether this chaperone protein is necessary for the toxicity of Aβ-GFP chimeric proteins. As indicated in Table 1 and supplementary material Fig. S2, deletion of *HSP104* partially restored the viability of cells expressing MFα-Aβ$_{42}$-GFP and MFα-Aβ$_{ARC}$-GFP. This result was unexpected because Hsp104p is a cytosolic protein and MFα-Aβ$_{42}$-GFP and MFα-Aβ$_{ARC}$-GFP were associated with the secretory pathway. We therefore conclude that some of the toxic species formed by Aβ-GFP chimeric proteins become cytosolic. This is consistent with the observation that the mature form detected by western blot analysis is sensitive to proteinase K (Fig. 3C).

In the *Δhsp104* strain, the fluorescent profile of Aβ-GFP chimeric proteins was filamentous and no foci were observed (Fig. 6). These results suggest that Hsp104p plays a role in the toxicity of MFα-Aβ$_{ARC}$-link-GFP, probably by favoring the conversion of big aggregates into smaller and toxic ones.

Respiratory rate of cells expressing MFα-Aβ$_{ARC}$-link-GFP is affected

Mitochondrial dysfunction plays a key role in AD. We therefore tested whether the toxicity triggered by the expression of Aβ-GFP chimeric proteins in yeast was associated with a mitochondrial disorder. To this end, we monitored the growth and consumption of oxygen in aerobic conditions at different time points after Aβ induction. Yeast cells transformed with the chimeric constructions

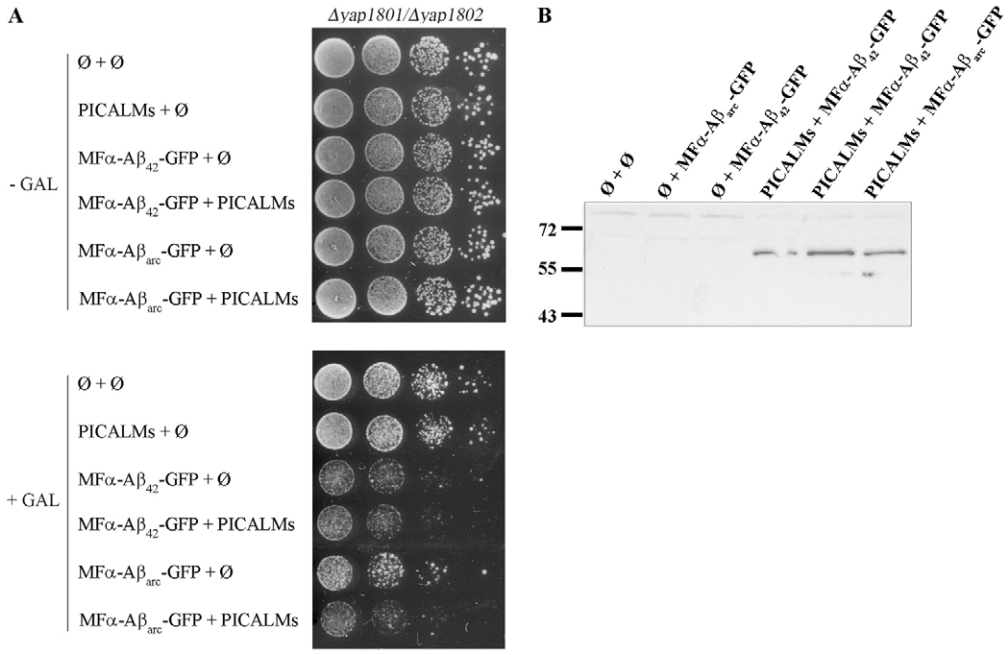

Fig. 5. Mammalian PICALM enhances the toxicity of Aβ in yeast. (A) Tenfold dilutions of exponentially growing cultures of BY4742 cells transformed with plasmids carrying the different chimeric constructions under the GAL10 promoter and, as indicated, a plasmid containing or not the short form of the PICALM cDNA under the GAL10 promoter were spotted on the same plate onto SD (–) or SG (+) agar supplemented with 20 mg/l histidine, 20 mg/l lysine and 60 mg/l leucine. (B) Deleted strains expressing the different chimeric proteins (6 hours of expression) with or without PICALM protein were collected for total-protein extraction. Proteins were separated by SDS-PAGE on a 12% polyacrylamide gel, transferred onto a nitrocellulose membrane and then exposed to polyclonal anti-PICALM antibodies (CALM H-134; Santa Cruz Biotechnology).

were grown with lactate as a carbon source and addition of 0.2% galactose at the mid-log phase to induce expression of the chimeric protein. Under these conditions, the growth of cells expressing MFα-GFP or MFα-$Aβ_{ARC}$-link-GFP was the same as that for cells carrying an empty vector during the first 4 hours of the induction. After this time, the growth rate of cells expressing the two chimeric proteins slowed, and this slowdown was stronger for cells expressing MFα-$Aβ_{ARC}$-link-GFP (Fig. 7A). We then evaluated the respiratory rate of the cells at different times during Aβ induction (Fig. 7B). The consumption of oxygen by cells with an empty vector or expressing MFα-GFP was unchanged 4 hours after induction (addition of galactose). By contrast, the respiratory rate decreased in the cells expressing MFα-$Aβ_{ARC}$-link-GFP. This reduction in oxygen consumption was higher after 8 hours of induction, whereas the respiratory rates of the two controls (empty vector and MFα-GFP) decreased only by a small amount in both cases. This difference was not due to cell lethality because the viability (measured by the number of colonies formed after plating) was the same after 8 hours of induction (data not shown). Such decline of oxygen consumption can be due either to a decrease in mitochondria contents or to a defect in the electron transport chain. We measured the mitochondrial content by recording the optical absorption spectra of mitochondrial cytochromes. The concentration of these different cytochromes is not specifically changed during Aβ expression (Fig. 7C), as expected if the deleterious effect depends on the inhibition of the respiratory chain.

DISCUSSION

Aβ must enter the secretory pathway to become toxic

In well-established model organisms such as *Caenorhabditis elegans* (Link, 1995) or *Drosophila melanogaster* (Crowther et al., 2005; Iijima et al., 2004), Aβ is always expressed in frame with a signal peptide. This expression is thought to represent the mammalian situation and is expected to yield extracellular Aβ. These models have shown that physiological impairments can happen before the occurrence of large extracellular deposits and are instead correlated with the intracellular accumulation of Aβ in worm (Fay et al., 1998) and fly (Crowther et al., 2005). Consistent with these findings, the transgenic mouse AD model (Tg2576) displayed defects in morphology, behavior and memory months before $Aβ_{42}$ plaque deposition was apparent (Jacobsen et al., 2006). In addition, plaque prevalence does not strictly correlate with dementia in AD (Schmitt et al., 2000; Davies et al., 1988). All of these results imply a pivotal role for intracellular Aβ, but its production is always puzzling because the protein is directed towards the extracellular space. Despite the usefulness of model organisms, there are no published reports that specifically address the role of the secretory pathway in generating toxic amyloid species. In the present study, we confirm that Aβ (expressed alone or stabilized by the GFP tag) produced in the cytoplasm does not significantly impair yeast growth. In our hands, and even under harsher conditions (37°C), yeast growth was comparable regardless of whether $Aβ_{1-42}$, $Aβ_{ARC}$, or GFP alone was expressed. By contrast, translocation of the same species into the secretory pathway could dramatically altered their toxicity. Our results are in complete agreement with those published recently in a yeast system (Treusch et al., 2011).

Chimeric Aβ-GFP are relevant for toxicity study

Our biological system is based on translational fusion between Aβ and GFP. With this system, the results are opposite to those of a study recently published in which PICALM orthologous genes protect from Aβ toxicity (Treusch et al., 2011). In this model, Aβ is supposed to transit through the secretory pathway to the plasma membrane. Aβ toxicity is observed only when a huge amount of this peptide is produced. This high production results both from insertion of multiple tandem copies and codon optimization for expression in yeast. At a lower level of expression (one integrated

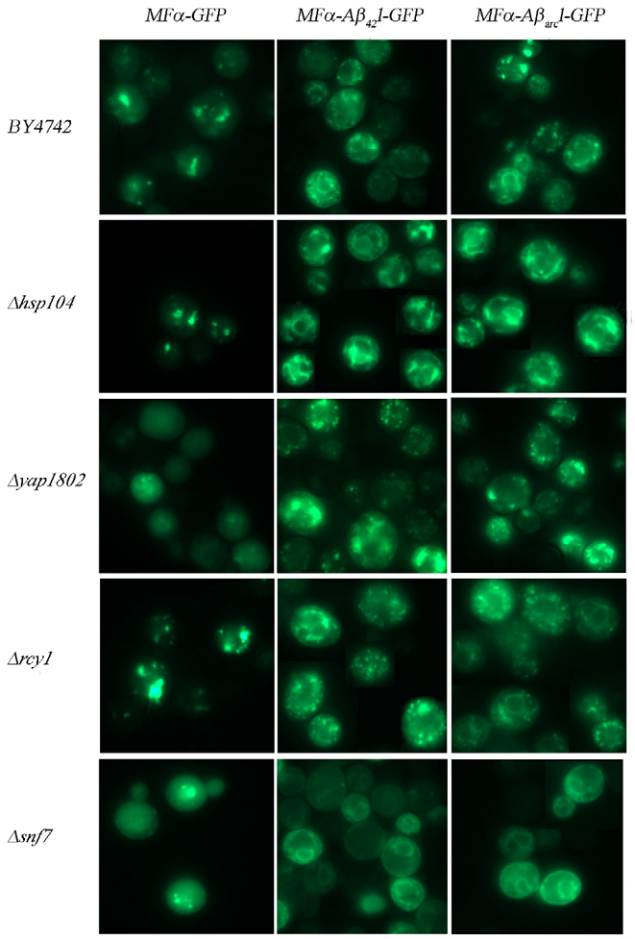

Fig. 6. GFP pattern of aggregation in yeast mutants. Wild-type or strains deleted for *YAP1802*, *HSP104*, *RCY1* or *SNF7* were grown for 6 hours in SG liquid medium supplemented with 0.67% casamino acids to induce expression of the chimeric proteins and were then examined by epifluorescence microscopy.

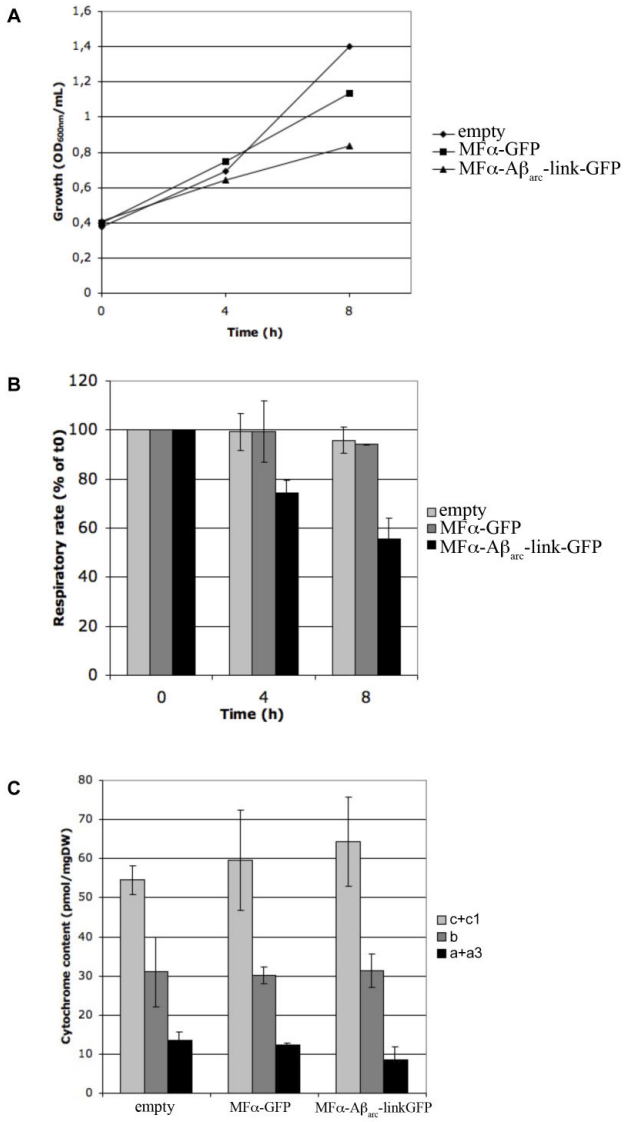

Fig. 7. Aβ expression leads to a decrease in O_2 consumption without changing cytochrome content. (A) BY4742 cells transformed with an empty vector (empty) or plasmids carrying the different chimeric constructions under the GAL10 promoter (MFα-GFP and MFα-$Aβ_{ARC}$-link-GFP) were grown aerobically in medium containing 2% DL-lactate and 0.2% galactose. (B) Respiratory rates of BY4742 cells transformed with an empty vector (empty) or plasmids carrying the different chimeric constructions under the GAL10 promoter (MFα-GFP and MFα-$Aβ_{ARC}$-link-GFP) (C) Cytochrome content of transformed BY4742 cells at 8 hours after induction. Results are mean ± s.d. of at least two measurements performed on two independent cell cultures.

copy), Aβ toxicity cannot be detected anymore (supplementary material Fig. S1) (Treusch et al., 2011). Interestingly, the results found with this system were validated in *C. elegans* and rat hippocampal neurons. In these three models, cells are also exposed to huge amount of Aβ produced into the ER or added in the medium as pre-formed oligomeric Aβ species. By contrast, when we expressed Aβ without GFP, we got a modest toxic effect. These results indicate that PICALM might protect cells in the presence of large amounts of Aβ, but it does not rule out the possibility that the same properties (increasing endocytosis) might lead to an opposite effect when Aβ concentration is below some threshold value. In our system, the MFα pre-sequence warrants us to follow the efficient entry and processing into the secretory pathway because this sequence is glycosylated and cleaved in the trans-Golgi. It might also change the aggregative properties of Aβ that behaves, during this traffic, as part of the cargo protein and mimics its properties during APP trafficking. We think that this difference from the other yeast system might also explain some discrepancies. The presence of a folded protein, such as the functional domain of the yeast translation termination factor Sup35p, downstream of Aβ does not change the ability of the natural peptide to aggregate (Bagriantsev and Liebman, 2006). We cannot rule out the possibility that the presence of GFP might interfere with the aggregative properties of Aβ, but this presence does not change the relative toxic properties of Aβ (wild-type versus arctic). As Aβ-GFP enters the secretory pathway, such toxicity could be due to a saturation of the ER-associated degradation (ERAD) system. By determining the expression of a reporter gene, we found that the unfolded

protein response (UPR) is higher when GFP is secreted alone (data not shown), though it is less toxic. In addition, MFα-$Aβ_{ARC}$-GFP is more toxic than MFα-Aβ-GFP and both species are expressed at the same level. It is therefore clear that the toxicity is due to a qualitative effect rather than induced by an overwhelming UPR. This conclusion is consistent with our experiment based on mutants acting downstream to the ER translocation; the toxicity in some of these mutants was clearly lower, indicating that crucial steps for deleterious effects are required in addition to the translocation event.

The yeast model gives new insight for the role of PICALM in AD

Recent genome-wide association studies have identified new genetic risk factors for AD. These studies have focused our attention on *PICALM*, which was identified independently by different groups as a locus associated with AD risk (Lambert et al., 2011; Harold et al., 2009). In contrast with other genes such as *APOE*, *CLU* and *CR1*, which are also risk factors for AD and for which much data is available in the context of AD, little is known about *PICALM*. The Yap180 proteins include Yap1801p and Yap1802p, which are the yeast homologs of PICALM (Wendland and Emr, 1998). Like PICALM, these proteins are involved in the assembly of clathrin cages at sites of formation of endocytic vesicles. Deletions of one or both genes encoding these proteins reduce the toxicity of Aβ. This decrease in toxicity was clearly reversed when mouse PICALM was expressed in yeast, demonstrating a direct role of the corresponding proteins in Aβ toxicity. In a different yeast model (Treusch et al., 2011), PICALM has the opposite effect. Their finding led Treusch et al. to conclude that Aβ expression led to a deficiency in clathrin-mediated endocytosis that could be reversed by YAP overexpression. However, this idea must be tempered by the fact that this mechanism is not essential in yeast and that its failure does not lead to an altered growth phenotype, at least in normal growth conditions. Finally, the functional characterization of PICALM mutations associated with an increase in AD risk will allow the determination of the exact role of this protein in Aβ toxicity.

Translocated and non-translocated Aβ forms distinct cytoplasmic aggregates

We established that almost all of the synthesized prepro-Aβ-GFP enters the secretory pathway. The 41-kDa species (corresponding to the unglycosylated form of prepro-Aβ-GFP) appeared only as a faint band during western blot analysis. This band was also barely detectable in the *ΔKEX2* strain whereas it was the predominant species following deglycosylation treatment of the crude extract. These biochemical properties are consistent with the GFP profile exhibiting a clear ER pattern. Prepro-Aβ-GFP is thus not diverted to the cytoplasm (or only an extremely small amount is diverted). This putative traffic, if it exists, might be antagonized by selective degradation of the species, but the net result would be the same, i.e. almost all of the detectable protein goes into the secretory pathway. Despite being correctly processed into the secretory pathway, most of the Aβ peptide is not secreted into the liquid medium, but is retained within the cell. Some mutants showed a clear accumulation of chimeric GFP proteins at the plasma membrane. The protein is thus transported within membrane vesicles to the periphery of the yeast cells. Secreted Aβ-GFP is processed by the glycosylation machinery and is finally released into the lumen of the secretory vesicle budding from the trans-Golgi network, where Kex2p is localized (Redding et al., 1991). Aggregation of the protein might occur when Aβ is still linked to its pre-sequence. However, such aggregation could impair Kex2p processing and it therefore seems reasonable to postulate that aggregation will occur only after cleavage of the pre-sequence. We found that Aβ toxicity was partially controlled by Hsp104. Hsp104 is a cytoplasmic chaperone that solubilizes large aggregates into smaller species and has been reported to inhibit the fibrillization of monomeric and protofibrillar forms of Aβ in vitro (Arimon et al., 2008). The function of Hsp104 in Aβ toxicity is probably direct, leading to the production of smaller entities that might be toxic to yeast cells. This result argues for a cytoplasmic localization of the toxic species. This intracellular localization is somewhat surprising given that the $Aβ_{42}$ constructs are based on a signal sequence that should have led to the extracellular release of $Aβ_{42}$. The same Aβ-GFP chimeric proteins behave differently when expressed directly in the cytoplasm (formation of foci and not toxic) or in the secretory pathway (undetectable under fluorescence microscope and toxic). The presence of a linker between Aβ and GFP restores the fluorescence of the secreted protein and we therefore postulate that the lack of fluorescence is due to a particular aggregation of the Aβ moiety when the protein is secreted. It is already known that partners that aggregate into insoluble material interfere with the ability of GFP to achieve its native fluorescent structure (Waldo et al., 1999). This property has been used to search for Aβ variants with reduced tendencies to aggregate (Wurth et al., 2002). Our results suggest that the cytoplasmic aggregates formed by the secreted Aβ are different from the aggregates formed during cytoplasmic expression of Aβ (without the signal sequence).

With our yeast model, we were able to expand our finding and to demonstrate that the endocytosis and recycling pathways are involved in Aβ toxicity. In the yeast model, this effect would change the rising of toxic species produced during vesicle transport between the plasma membrane and the Golgi. These species would then escape from the membrane compartment. It has been recently shown in a cellular model that bundles of Aβ fibrils formed from soluble extracellular Aβ penetrate the vesicular membrane and extend into the cytoplasm prior to cell death (Friedrich et al., 2010). The same mechanism in yeast could yield cytoplasmic aggregates. Such aggregates could be then taken in charge by Hsp104. In the absence of this disaggregase, the equilibrium would be in favor of large and nontoxic aggregates. By contrast, the presence of Hsp104 would increase the ratio of small and toxic aggregates to larger aggregates. These species would then interact with cellular compartments such as mitochondria. In our model, the change of oxygen consumption was observed very early after Aβ expression. Because *S. cerevisiae* is a facultative anaerobe, mitochondrial integrity might have been affected without any dramatic change in cell viability. However, the same events could have more severe consequences in mammalian cells.

Our study provides convincing arguments for the use of yeast cells as a cellular model for scoring Aβ toxicity. Our yeast system is now suitable for screening procedures and will enable many different leads in the search for chemical or genetic modifiers of Aβ toxicity. Our study also offers a conceptual framework to highlight the role of PICALM and endocytosis in cellular injury and confirms the capacity of Aβ to cross cellular membranes. This

initial analysis paves the way for further research that should be as powerful as that used to define molecular mechanisms underlying other amyloid related diseases.

METHODS

Yeast strains and media

Yeast strains (listed in supplementary material Table S1) were transformed with plasmids carrying the different chimeric constructs under the GAL10 promoter and were grown overnight on dextrose medium (0.67% yeast nitrogen base, 2% dextrose) supplemented with 0.67% casamino acids or with some of the following amino acids: 20 mg/l histidine (H), 20 mg/l lysine (K) and 60 mg/l leucine (L). Upon reaching exponential phase (OD_{600}=1), the cells were placed in galactose medium supplemented with either 0.67% casamino acids or HKL to induce the expression of chimeric proteins. After 6 hours, cells were either collected to obtain total cell extracts or were observed under epifluorescence.

The *Δyap1801/1802* strain was constructed by mating the two simple deleted strains Δ*yap1801* and Δ*yap1802*. The mating type of the Δ*yap1801* strain was changed by transforming the strain with a plasmid carrying the *HO* gene. The two strains were then crossed by patching them mixed on a selective medium. After verifying mating by microscopy, the diploid strain was patched onto a sporulation medium. After 3 days of growth, tetrads were dissected and the resistance of the spores to G418 was tested. The G418-resistant spores from the double recombined tetrads were kept as *Δyap1801/1802* strains. To lose the plasmid carrying the *HO* gene, *Δyap1801/1802* was then plated onto rich medium containing 5FOA.

Oligonucleotides are listed in supplementary material Table S2. The $Aβ_{1-42}$ sequence was amplified by PCR from pSG5-APP (a kind gift from Agnès Hémar) using oligonucleotide 792, which introduces a *Bam*HI restriction site at the 5′ end of the fragment and an ATG codon at the beginning of the $Aβ_{1-42}$ sequence, and oligonucleotide 794. The PCR fragment was then inserted into the plasmid pYecHetsYGFP (Couthouis et al., 2009), which had been previously linearized by *Bam*HI using a gap repair method (Orr-Weaver and Szostak, 1983). The pYeαAβYGFP and $pYeαAβ_{ARC}$YGFP plasmids were constructed by cloning a synthetic sequence in a *Bam*HI-*Bst*XI-digested pYeAβYGFP plasmid. These synthetic sequences, made by GeneScript, were composed of *Bam*HI restriction site followed by α-factor prepro sequence, Aβ wild-type or arctic mutant coding sequence, the 5′ end of the GFP sequence, and a *Bst*XI restriction site. The $pYeAβ_{ARC}$YGFP plasmid was created by overlapping PCR using $pYeαAβ_{ARC}$YGFP as a template (with oligonucleotides 705, 706, 859 and 860). This allowed the amplification of a P_{GAL}-$Aβ_{ARC}$-GFP fragment, which was introduced by a gap repair method into a *Bam*HI-*Bst*XI-digested $pYeαAβ_{ARC}$YGFP plasmid. Similarly, P_{GAL}-α-factor prepro-GFP and P_{GAL}-GFP sequences were created by overlapping PCR using pYeαAβYGFP and pYeAβYGFP as templates (with oligonucleotides 705, 706, 856, 857 and 858). The fragments were respectively inserted into pYeαAβYGFP and pYeAβGFP *Bam*HI-*Bst*XI-digested plasmids. Each of these plasmids is a multicopy yeast-expression plasmid with the URA3 selectable marker and a *GAL10* promoter in a pYeHFN2U backbone (Cullin and Minvielle-Sebastia, 1994). CALM long splice variant (CALM-L; GenBank ID BC011470) and short splice variant (CALM-S; GenBank ID BC021491) from the American Tissue Culture Collection (ATCC) were amplified by PCR using oligonucleotide 951, which introduced a *Bam*HI site at the 5′ end of the cDNA and oligonucleotide 952 which introduced a *Not*I site at the 3′ end of the cDNA. After digestion by *Bam*HI and *Not*I, the PCR fragment was inserted into the pYeHFN2L plasmid. This plasmid is a multicopy yeast-expression plasmid with an LEU2 selectable marker and a *GAL10* promoter (Cullin and Minvielle-Sebastia, 1994).

Spotting assay

All spotting assays were performed under the same conditions. Tenfold serial dilutions starting with an equal number of cells (1 OD; where 1=600 nm) were performed in sterile water. Spotting assays were derived from a pool of three independent fresh transformants. Drops of 10 µl were then plated onto the appropriate SD or SG medium.

Fluorescence microscopy

Cells were washed in water and resuspended in medium. An Axioskop 2 plus (Zeiss) fluorescence microscope was coupled with an AxioCam (Zeiss) black and white camera. The following filters were used: LP-GFP (GFP) and N3 (RFP).

Protein extraction, deglycosylation and western blotting

The alkaline lysis method was used for protein extraction. Briefly, 5 OD units of yeast cells in exponential growth phase were permeabilized with 500 µl of 0.185 M NaOH, and 0.2% β-mercaptoethanol. After 10 minutes of incubation on ice, trichloroaceticacid (TCA) was added to obtain a final concentration of 5%, and the samples were incubated for an additional 10 minutes on ice. Precipitates were then collected by centrifugation at 13,000 ***g*** for 5 minutes. Pellets were dissolved in 35 µl of dissociation buffer (4% sodium dodecyl sulfate, 0.1 M Tris-HCl pH 6.8, 4 mM EDTA, 20% glycerol, 2% 2-mercaptoethanol and 0.02% Bromophenol Blue) and 15 µl of 1 M Tris-base. For deglycosylation assays, pellets were suspended in 20 µl glycoprotein denaturing buffer (Biolabs), incubated for 10 minutes at 100°C, and transferred for a few minutes at 4°C. We then added 5 µl 10× G7 reaction buffer, 5 µl 10% NP40 and 5 µl deglycosylation enzyme cocktail (PNGase F, 500,000 U/ml; endo-α-*N*-acetylgalactosaminidase, 400,000,000 U/ml; neuraminidase, 50,000 U/ml; β1-4 galactosidase, 8000 U/ml; and β-*N*-acetylglucosaminidase, 4000 U/ml) to obtain a volume of 50 µl. The samples were then incubated for 4 hours at 37°C before adding 15 µl of sample buffer.

Yeast proteins were incubated for 5 minutes at 100°C and separated by SDS-PAGE in a 12% polyacrylamide gel. Proteins were electrically transferred onto nitrocellulose membranes (Optitran BA-S83; Schleicher and Schuell) in the presence of transfer buffer (39 mM glycine, 48 mM Tris-base, 2% EtOH and 0.037% SDS) and were probed with monoclonal anti-GFP antibodies (Sigma) or anti-Aβ (Tebu) antibodies. Peroxidase-conjugated anti-mouse antibodies (Sigma) were used as secondary antibodies. Binding was detected with the SuperSignal reagent (Pierce) and the VersaDoc Imaging system (BioRad).

Fractionation and proteinase K treatment

250 OD yeast culture in exponential growth phase in SG medium supplemented with 0.67% casamino acids was collected by

centrifugation (4000 ***g***), washed in 20 ml H_2O and resuspended in 12 ml of spheroplasting buffer (1.4 M sorbitol, 50 mM Tris-Cl pH 7.5, 40 mM 2-mercaptoethanol and 0.4 mg/ml zymolyase 20T) and incubated for 20 minutes at 30°C without shaking. Spheroplasts were centrifuged for 3 minutes at 1500 ***g*** at 4°C. The pellet was resuspended in 20 ml of cold lysis buffer (20 mM triethanolamine, 1 mM EDTA pH 7.2, 0.8 M sorbitol, 2 mM phenylmethylsulfonyl fluoride and 5 mg/ml each of leupeptin, chymostatin, aprotinin, pepstatin A and antipain). The spheroplasts were then lysed with a Dounce homogenizer (20 strokes). Lysates were cleared by centrifugation at 500 ***g*** for 5 minutes at 4°C and the supernatant centrifuged at 13,000 ***g*** for 10 minutes. The P13 fraction was then used for protease protection assays. P13 fractions were resuspended in lysis buffer and incubated with combinations of 0.3125 mg/ml proteinase K (Roche) and/or 5% Triton X-100 for 30 minutes at 30°C with gentle shaking. The reactions were then stopped with 10% TCA for 10 minutes at 4°C. Samples were then centrifuged at 13,000 ***g*** for 10 minutes at 4°C and the pellets suspended in 10 µl protein sample buffer and separated by SDS-PAGE.

Oxygen consumption assays

Cells were grown aerobically at 28°C in the following medium: 0.175% yeast nitrogen base, 0.5% $(NH_4)_2SO_4$, 0.1% KH_2PO_4, 0.2% DL-lactate (w/v), pH 5.5. Respiration assays of growing cells were performed in the growth medium. Samples of cells were harvested throughout the growth period, washed twice in distilled water and their dry-weight determined. Oxygen consumption was measured polarographically at 28°C using a Clark oxygen electrode in a 1-ml thermostatically controlled chamber. Respiratory rates (JO_2) were determined from the slope of a plot of O_2 concentration versus time and were expressed as natO/minute/mg dry weight.

For determination of cytochrome content, cells were harvested after 8 hours, washed twice with distilled water and concentrated to obtain 2 ml of a cell suspension of about 50 OD units at 600 nm. They were placed in a dual spectrophotometer (Aminco DW2000) and a differential spectrum (from 500 to 650 nm) was obtained from 1 ml of cells in the presence of 1 µl of 70% H_2O_2 (w/v) (oxidized state) and 1 ml of cells in the presence of a few grains of dithionite (reduced state). Calculations of cytochrome c+c1 and cytochrome b contents were performed using an extinction coefficient of 18,000 $M^{-1}cm^{-1}$ for the wavelength pairs 550-540 nm and 561-575 nm, respectively. The calculation of cytochrome a+a3 contents was performed using an extinction coefficient of 12,000 $M^{-1}cm^{-1}$ for the 603-630 nm interval.

ACKNOWLEDGEMENTS

Axel Edelman and Co. have proofread the manuscript.

COMPETING INTERESTS

The authors declare that they do not have any competing or financial interests.

AUTHOR CONTRIBUTIONS

F.D.A. and H.V. performed all of the experiments apart from the EM experiments, which were performed by B.S. J.D.M. set up the centrifugation assays and PK analysis and contributed to scientific discussions. A.D. supervised the respiratory analysis. C.M. and C.C. conceived and partially performed the work and wrote the paper.

FUNDING

F.D.A. was supported by a grant from le Ministère de la Recherche.

SUPPLEMENTARY MATERIAL

Supplementary material for this article is available at http://dmm.biologists.org/lookup/suppl/doi:10.1242/dmm.010108/-/DC1

REFERENCES

Almeida, C. G., Takahashi, R. H. and Gouras, G. K. (2006). Beta-amyloid accumulation impairs multivesicular body sorting by inhibiting the ubiquitin-proteasome system. *J. Neurosci.* **26**, 4277-4288.

Arimon, M., Grimminger, V., Sanz, F. and Lashuel, H. A. (2008). Hsp104 targets multiple intermediates on the amyloid pathway and suppresses the seeding capacity of Abeta fibrils and protofibrils. *J. Mol. Biol.* **384**, 1157-1173.

Babst, M., Katzmann, D. J., Estepa-Sabal, E. J., Meerloo, T. and Emr, S. D. (2002). Escrt-III: an endosome-associated heterooligomeric protein complex required for mvb sorting. *Dev. Cell* **3**, 271-282.

Bagriantsev, S. and Liebman, S. (2006). Modulation of Abeta42 low-n oligomerization using a novel yeast reporter system. *BMC Biol.* **4**, 32.

Burston, H. E., Maldonado-Báez, L., Davey, M., Montpetit, B., Schluter, C., Wendland, B. and Conibear, E. (2009). Regulators of yeast endocytosis identified by systematic quantitative analysis. *J. Cell Biol.* **185**, 1097-1110.

Caine, J., Sankovich, S., Antony, H., Waddington, L., Macreadie, P., Varghese, J. and Macreadie, I. (2007). Alzheimer's Abeta fused to green fluorescent protein induces growth stress and a heat shock response. *FEMS Yeast Res.* **7**, 1230-1236.

Cooper, A. A., Gitler, A. D., Cashikar, A., Haynes, C. M., Hill, K. J., Bhullar, B., Liu, K., Xu, K., Strathearn, K. E., Liu, F. et al. (2006). Alpha-synuclein blocks ER-Golgi traffic and Rab1 rescues neuron loss in Parkinson's models. *Science* **313**, 324-328.

Costaguta, G., Duncan, M. C., Fernández, G. E., Huang, G. H. and Payne, G. S. (2006). Distinct roles for TGN/endosome epsin-like adaptors Ent3p and Ent5p. *Mol. Biol. Cell* **17**, 3907-3920.

Couthouis, J., Rébora, K., Immel, F., Berthelot, K., Castroviejo, M. and Cullin, C. (2009). Screening for toxic amyloid in yeast exemplifies the role of alternative pathway responsible for cytotoxicity. *PLoS ONE* **4**, e4539.

Crowther, D. C., Kinghorn, K. J., Miranda, E., Page, R., Curry, J. A., Duthie, F. A., Gubb, D. C. and Lomas, D. A. (2005). Intraneuronal Abeta, non-amyloid aggregates and neurodegeneration in a Drosophila model of Alzheimer's disease. *Neuroscience* **132**, 123-135.

Cullin, C. and Minvielle-Sebastia, L. (1994). Multipurpose vectors designed for the fast generation of N- or C-terminal epitope-tagged proteins. *Yeast* **10**, 105-112.

Davies, L., Wolska, B., Hilbich, C., Multhaup, G., Martins, R., Simms, G., Beyreuther, K. and Masters, C. L. (1988). A4 amyloid protein deposition and the diagnosis of Alzheimer's disease: prevalence in aged brains determined by immunocytochemistry compared with conventional neuropathologic techniques. *Neurology* **38**, 1688-1693.

Echeverria, V., Ducatenzeiler, A., Alhonen, L., Janne, J., Grant, S. M., Wandosell, F., Muro, A., Baralle, F., Li, H., Duff, K. et al. (2004). Rat transgenic models with a phenotype of intracellular Abeta accumulation in hippocampus and cortex. *J. Alzheimers Dis.* **6**, 209-219.

Fay, D. S., Fluet, A., Johnson, C. J. and Link, C. D. (1998). In vivo aggregation of beta-amyloid peptide variants. *J. Neurochem.* **71**, 1616-1625.

Finelli, A., Kelkar, A., Song, H.-J., Yang, H. and Konsolaki, M. (2004). A model for studying Alzheimer's Abeta42-induced toxicity in Drosophila melanogaster. *Mol. Cell. Neurosci.* **26**, 365-375.

Fonte, V., Kapulkin, V., Taft, A., Fluet, A., Friedman, D. and Link, C. D. (2002). Interaction of intracellular beta amyloid peptide with chaperone proteins. *Proc. Natl. Acad. Sci. USA* **99**, 9439-9444.

Franssens, V., Boelen, E., Anandhakumar, J., Vanhelmont, T., Büttner, S. and Winderickx, J. (2010). Yeast unfolds the road map toward alpha-synuclein-induced cell death. *Cell Death Differ.* **17**, 746-753.

Friedrich, R. P., Tepper, K., Rönicke, R., Soom, M., Westermann, M., Reymann, K., Kaether, C. and Fändrich, M. (2010). Mechanism of amyloid plaque formation suggests an intracellular basis of Abeta pathogenicity. *Proc. Natl. Acad. Sci. USA* **107**, 1942-1947.

Fushimi, K., Long, C., Jayaram, N., Chen, X., Li, L. and Wu, J. Y. (2011). Expression of human FUS/TLS in yeast leads to protein aggregation and cytotoxicity, recapitulating key features of FUS proteinopathy. *Protein Cell* **2**, 141-149.

Galan, J. M., Wiederkehr, A., Seol, J. H., Haguenauer-Tsapis, R., Deshaies, R. J., Riezman, H. and Peter, M. (2001). Skp1p and the F-box protein Rcy1p form a non-SCF complex involved in recycling of the SNARE Snc1p in yeast. *Mol. Cell. Biol.* **21**, 3105-3117.

Hansson Petersen, C. A., Alikhani, N., Behbahani, H., Wiehager, B., Pavlov, P. F., Alafuzoff, I., Leinonen, V., Ito, A., Winblad, B., Glaser, E. et al. (2008). The amyloid beta-peptide is imported into mitochondria via the TOM import machinery and localized to mitochondrial cristae. *Proc. Natl. Acad. Sci. USA* **105**, 13145-13150.

Harold, D., Abraham, R., Hollingworth, P., Sims, R., Gerrish, A., Hamshere, M. L., Pahwa, J. S., Moskvina, V., Dowzell, K., Williams, A. et al. (2009). Genome-wide association study identifies variants at CLU and PICALM associated with Alzheimer's disease. *Nat. Genet.* **41**, 1088-1093.

Hoshino, T., Murao, N., Namba, T., Takehara, M., Adachi, H., Katsuno, M., Sobue, G., Matsushima, T., Suzuki, T. and Mizushima, T. (2011). Suppression of Alzheimer's disease-related phenotypes by expression of heat shock protein 70 in mice. *J. Neurosci.* **31**, 5225-5234.

Hu, X., Crick, S. L., Bu, G., Frieden, C., Pappu, R. V. and Lee, J. M. (2009). Amyloid seeds formed by cellular uptake, concentration, and aggregation of the amyloid-beta peptide. *Proc. Natl. Acad. Sci. USA* **106**, 20324-20329.

Huh, W. K., Falvo, J. V., Gerke, L. C., Carroll, A. S., Howson, R. W., Weissman, J. S. and O'Shea, E. K. (2003). Global analysis of protein localization in budding yeast. *Nature* **425**, 686-691.

Iijima, K., Liu, H. P., Chiang, A. S., Hearn, S. A., Konsolaki, M. and Zhong, Y. (2004). Dissecting the pathological effects of human Abeta40 and Abeta42 in Drosophila: a potential model for Alzheimer's disease. *Proc. Natl. Acad. Sci. USA* **101**, 6623-6628.

Iijima-Ando, K., Hearn, S. A., Shenton, C., Gatt, A., Zhao, L. and Iijima, K. (2009). Mitochondrial mislocalization underlies Abeta42-induced neuronal dysfunction in a Drosophila model of Alzheimer's disease. *PLoS ONE* **4**, e8310.

Jacobsen, J. S., Wu, C. C., Redwine, J. M., Comery, T. A., Arias, R., Bowlby, M., Martone, R., Morrison, J. H., Pangalos, M. N., Reinhart, P. H. et al. (2006). Early-onset behavioral and synaptic deficits in a mouse model of Alzheimer's disease. *Proc. Natl. Acad. Sci. USA* **103**, 5161-5166.

Ju, S., Tardiff, D. F., Han, H., Divya, K., Zhong, Q., Maquat, L. E., Bosco, D. A., Hayward, L. J., Brown, R. H., Jr, Lindquist, S. et al. (2011). A yeast model of FUS/TLS-dependent cytotoxicity. *PLoS Biol.* **9**, e1001052.

Julius, D., Brake, A., Blair, L., Kunisawa, R. and Thorner, J. (1984). Isolation of the putative structural gene for the lysine-arginine-cleaving endopeptidase required for processing of yeast prepro-alpha-factor. *Cell* **37**, 1075-1089.

Kandimalla, K. K., Scott, O. G., Fulzele, S., Davidson, M. W. and Poduslo, J. F. (2009). Mechanism of neuronal versus endothelial cell uptake of Alzheimer's disease amyloid beta protein. *PLoS ONE* **4**, e4627.

Kurjan, J. and Herskowitz, I. (1982). Structure of a yeast pheromone gene (MF alpha): a putative alpha-factor precursor contains four tandem copies of mature alpha-factor. *Cell* **30**, 933-943.

Lambert, J. C., Zelenika, D., Hiltunen, M., Chouraki, V., Combarros, O., Bullido, M. J., Tognoni, G., Fiévet, N., Boland, A. et al. (2011). Evidence of the association of BIN1 and PICALM with the AD risk in contrasting European populations. *Neurobiol. Aging* **32**, e11-e15.

Langui, D., Girardot, N., El Hachimi, K. H., Allinquant, B., Blanchard, V., Pradier, L. and Duyckaerts, C. (2004). Subcellular topography of neuronal Abeta peptide in APPxPS1 transgenic mice. *Am. J. Pathol.* **165**, 1465-1477.

Li, J., Xu, H., Bentley, W. E. and Rao, G. (2002). Impediments to secretion of green fluorescent protein and its fusion from Saccharomyces cerevisiae. *Biotechnol. Prog.* **18**, 831-838.

Link, C. D. (1995). Expression of human beta-amyloid peptide in transgenic Caenorhabditis elegans. *Proc. Natl. Acad. Sci. USA* **92**, 9368-9372.

Magrané, J., Smith, R. C., Walsh, K. and Querfurth, H. W. (2004). Heat shock protein 70 participates in the neuroprotective response to intracellularly expressed beta-amyloid in neurons. *J. Neurosci.* **24**, 1700-1706.

Meriin, A. B., Zhang, X., He, X., Newnam, G. P., Chernoff, Y. O. and Sherman, M. Y. (2002). Huntington toxicity in yeast model depends on polyglutamine aggregation mediated by a prion-like protein Rnq1. *J. Cell Biol.* **157**, 997-1004.

Meyerholz, A., Hinrichsen, L., Groos, S., Esk, P. C., Brandes, G. and Ungewickell, E. J. (2005). Effect of clathrin assembly lymphoid myeloid leukemia protein depletion on clathrin coat formation. *Traffic* **6**, 1225-1234.

Nixon, R. A. (2007). Autophagy, amyloidogenesis and Alzheimer disease. *J. Cell Sci.* **120**, 4081-4091.

Orr-Weaver, T. L. and Szostak, J. W. (1983). Yeast recombination: the association between double-strand gap repair and crossing-over. *Proc. Natl. Acad. Sci. USA* **80**, 4417-4421.

Owen, D. J., Vallis, Y., Pearse, B. M., McMahon, H. T. and Evans, P. R. (2000). The structure and function of the beta 2-adaptin appendage domain. *EMBO J.* **19**, 4216-4227.

Rebeck, G. W., Hoe, H. S. and Moussa, C. E. (2010). Beta-Amyloid1-42 gene transfer model exhibits intraneuronal amyloid, gliosis, tau phosphorylation, and neuronal loss. *J. Biol. Chem.* **285**, 7440-7446.

Redding, K., Holcomb, C. and Fuller, R. S. (1991). Immunolocalization of Kex2 protease identifies a putative late Golgi compartment in the yeast Saccharomyces cerevisiae. *J. Cell Biol.* **113**, 527-538.

Schmitt, F. A., Davis, D. G., Wekstein, D. R., Smith, C. D., Ashford, J. W. and Markesbery, W. R. (2000). "Preclinical" AD revisited: neuropathology of cognitively normal older adults. *Neurology* **55**, 370-376.

Selkoe, D. J. and Podlisny, M. B. (2002). Deciphering the genetic basis of Alzheimer's disease. *Annu. Rev. Genomics Hum. Genet.* **3**, 67-99.

Shie, F.-S., LeBoeur, R. C. and Jin, L.-W. (2003). Early intraneuronal Abeta deposition in the hippocampus of APP transgenic mice. *Neuroreport* **14**, 123-129.

Sun, Z., Diaz, Z., Fang, X., Hart, M. P., Chesi, A., Shorter, J. and Gitler, A. D. (2011). Molecular determinants and genetic modifiers of aggregation and toxicity for the ALS disease protein FUS/TLS. *PLoS Biol.* **9**, e1000614.

Takahashi, R. H., Milner, T. A., Li, F., Nam, E. E., Edgar, M. A., Yamaguchi, H., Beal, M. F., Xu, H., Greengard, P. and Gouras, G. K. (2002). Intraneuronal Alzheimer abeta42 accumulates in multivesicular bodies and is associated with synaptic pathology. *Am. J. Pathol.* **161**, 1869-1879.

Treusch, S., Hamamichi, S., Goodman, J. L., Matlack, K. E., Chung, C. Y., Baru, V., Shulman, J. M., Parrado, A., Bevis, B. J. et al. (2011). Functional links between Aβ toxicity, endocytic trafficking, and Alzheimer's disease risk factors in yeast. *Science* **334**, 1241-1245.

von der Haar, T., Jossé, L., Wright, P., Zenthon, J. and Tuite, M. F. (2007). Development of a novel yeast cell-based system for studying the aggregation of Alzheimer's disease-associated Abeta peptides in vivo. *Neurodegener. Dis.* **4**, 136-147.

Waldo, G. S., Standish, B. M., Berendzen, J. and Terwilliger, T. C. (1999). Rapid protein-folding assay using green fluorescent protein. *Nat. Biotechnol.* **17**, 691-695.

Wendland, B. and Emr, S. D. (1998). Pan1p, yeast eps15, functions as a multivalent adaptor that coordinates protein-protein interactions essential for endocytosis. *J. Cell Biol.* **141**, 71-84.

Willingham, S., Outeiro, T. F., DeVit, M. J., Lindquist, S. L. and Muchowski, P. J. (2003). Yeast genes that enhance the toxicity of a mutant huntingtin fragment or alpha-synuclein. *Science* **302**, 1769-1772.

Wurth, C., Guimard, N. K. and Hecht, M. H. (2002). Mutations that reduce aggregation of the Alzheimer's Abeta42 peptide: an unbiased search for the sequence determinants of Abeta amyloidogenesis. *J. Mol. Biol.* **319**, 1279-1290.

Zhao, X. L., Wang, W. A., Tan, J. X., Huang, J. K., Zhang, X., Zhang, B. Z., Wang, Y. H., YangCheng, H. Y., Zhu, H. L. et al. (2010). Expression of beta-amyloid induced age-dependent presynaptic and axonal changes in Drosophila. *J. Neurosci.* **30**, 1512-522.

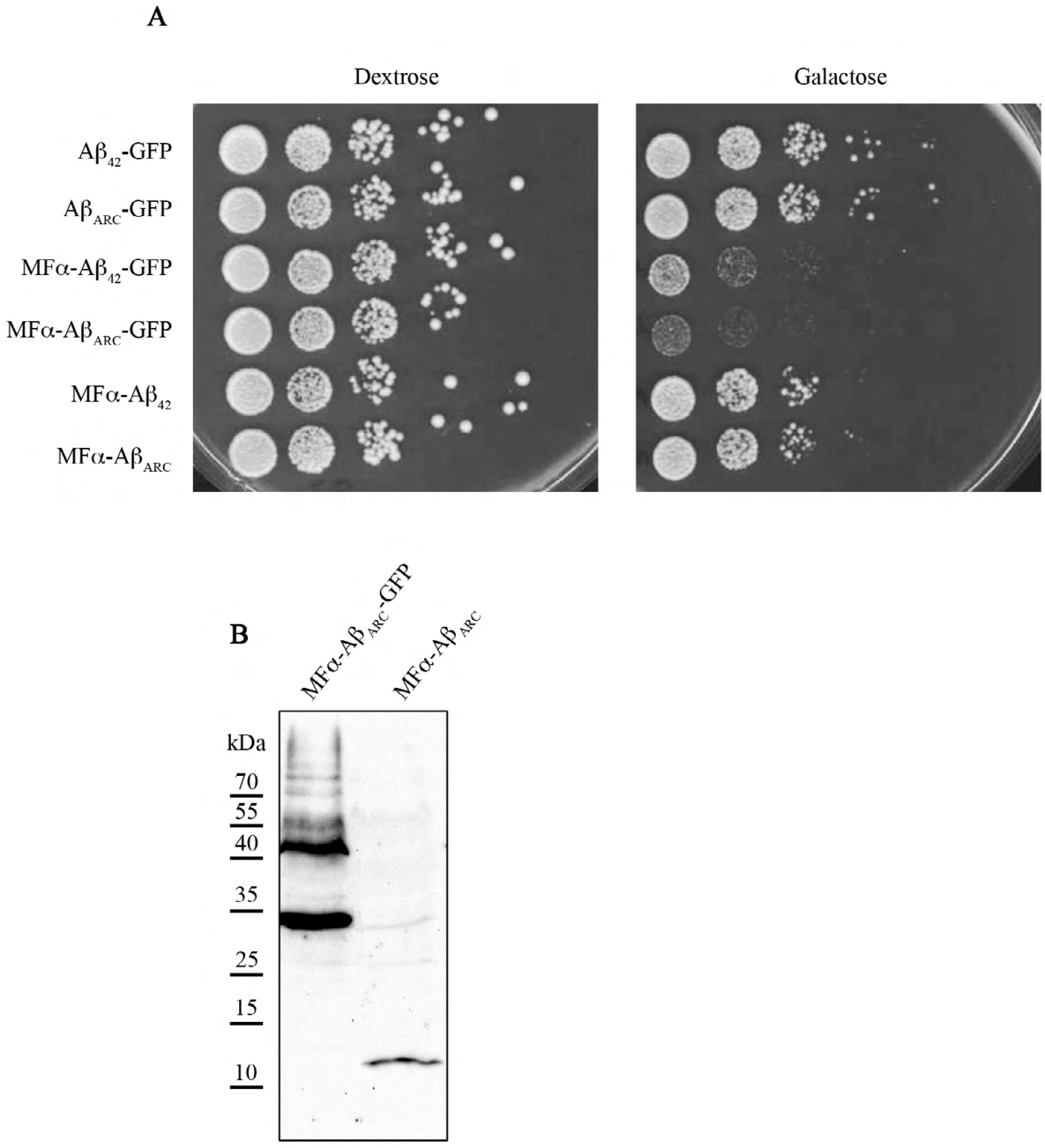

Fig. S1. Toxicity of Aβ alone. (A) Ten-fold dilutions of exponentially growing cultures of BY4742 cells transformed with plasmids carrying the different chimeric constructions under the GAL10 promoter were spotted onto SD (-) or SG (+) agar supplemented with 20 mg/l histidine, 20 mg/l lysine and 60 mg/l leucine. The cells were incubated at 30°C for 3 days. (B) BY4742 cells expressing the different chimeric proteins (6 hours of expression) were collected for total-protein extracts. Equal quantities of proteins were separated by SDS-PAGE on a 12% polyacrylamide gel, transferred onto a nitrocellulose membrane and exposed to anti-Aβ (Tebu) antibodies.

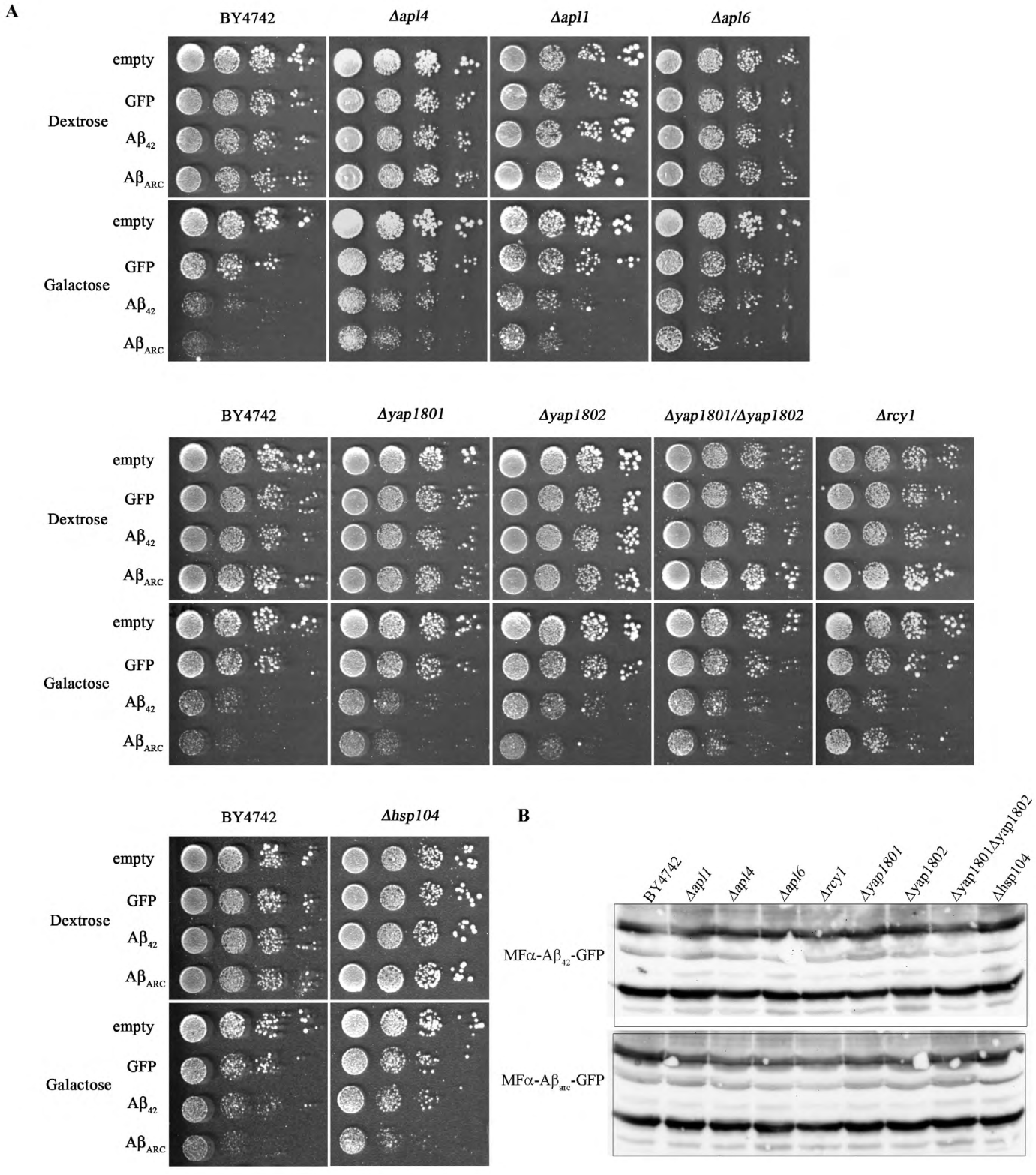

Fig. S2. Yeast mutants modulate Aβ toxixity without changing its protein level. (A) Ten-fold dilutions of exponentially growing cultures of deleted strains transformed with plasmids carrying the different chimeric constructions under the GAL10 promoter were spotted on the same plate onto SD (-) or SG (+) agar supplemented with 20 mg/l histidine, 20 mg/l lysine and 60 mg/l leucine. (B) Cells expressing the different chimeric proteins (6 hours of expression) were collected for total-protein extracts. Equal quantities of proteins were separated by SDS-PAGE on a 12% polyacrylamide gel, transferred onto a nitrocellulose membrane, and then exposed to monoclonal anti-GFP antibodies (Sigma).

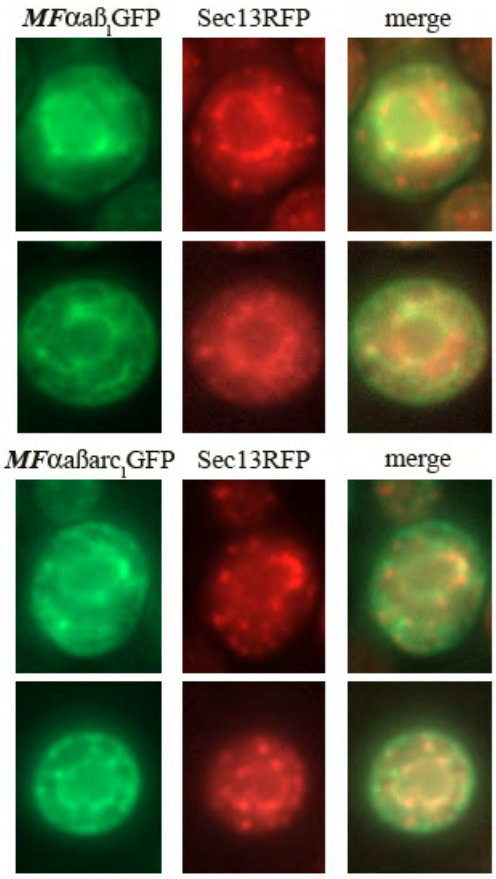

Fig. S3. Aβ-GFP species colocalize with ER. Wild-type or RFP-tagged strains were grown for 6 hours in SG liquid medium supplemented with 0.67% casaminoacids to induce the expression of the chimeric proteins and were then examined by epifluorescence microscopy.

Table 1. Yeast strains used in this study

Name of strain	Genotype	Source
BY4742	*MATa, his3Δ1, leu2Δ0, ura3Δ0*	Eurocarf yeast deletion library
Δ*apl4*	*MATa, his3Δ1, leu2Δ0, ura3Δ0, YPR029C::KanMX4*	Eurocarf yeast deletion library
Δ*apl1*	*MATa, his3Δ1, leu2Δ0, ura3Δ0, YJR005W::KanMX4*	Eurocarf yeast deletion library
Δ*apl2*	*MATa, his3Δ1, leu2Δ0, ura3Δ0, YKL135C::KanMX4*	Eurocarf yeast deletion library
Δ*apl3*	*MATa, his3Δ1, leu2Δ0, ura3Δ0, YBL037W ::KanMX4*	Eurocarf yeast deletion library
Δ*apm1*	*MATa, his3Δ1, leu2Δ0, ura3Δ0, YPL259C::KanMX4*	Eurocarf yeast deletion library
Δ*apm4*	*MATa, his3Δ1, leu2Δ0, ura3Δ0, YOL062C::KanMX4*	Eurocarf yeast deletion library
Δ*gga2*	*MATa, his3Δ1, leu2Δ0, ura3Δ0, YHR108W::KanMX4*	Eurocarf yeast deletion library
Δ*ent5*	*MATa, his3Δ1, leu2Δ0, ura3Δ0, YDR153C::KanMX4*	Eurocarf yeast deletion library
Δ*clc1*	*MATa, his3Δ1, leu2Δ0, ura3Δ0, YGR167W::KanMX4*	Eurocarf yeast deletion library
Δ*rcy1*	*MATa, his3Δ1, leu2Δ0, ura3Δ0, YJL204C::KanMX4*	Eurocarf yeast deletion library
Δ*yap1801*	*MATa, his3Δ1, leu2Δ0, ura3Δ0, YHR161C::KanMX4*	Eurocarf yeast deletion library
Δ*yap1802*	*MATa, his3Δ1, leu2Δ0, ura3Δ0, YGR241C::KanMX4*	Eurocarf yeast deletion library
Δ*hsp104*	*MATa, his3Δ1, leu2 Δ0, lys2 Δ0, ura3Δ0, YLL026W::KanMX4*	Eurocarf yeast deletion library
SEC13-RFP	*MATa, his3Δ1, leu2 Δ0, lys2 Δ0, ura3Δ0, YLR208W-RFP-KanMX6*	Peter Arvidson
Δ*yap1801/*Δ*yap1802*	*MATa, his3Δ1, leu2Δ0, ura3Δ0, YHR161C::KanMX4, YGR241C::KanMX4*	This study

Table S1. Yeast strains used in this study.

Table S2. Oligonucleotides used in this study

Number	Sequence
792	AAATACACACACTAAATTACCGGATCCTATGGATGCAGAATTCCGACATG
794	ACCAGTGAATAATTCTTCACCTTTAGACATCGCTATGACAACACCGCCCACC
705	GGATGGCCAGGCAACTTTAG
856	GAATAATTCTTCACCTTTAGACATAGCTTCAGCCTCTCTTTTATC
858	GAATAATTCTTCACCTTTAGACATGGATCCGGTAATTTAGTGTGT
859	GTCATGTCGGAATTCTGCATCCATGGATCCGGTAATTTAGTGTGT
706	TTTACACTTTATGCTTCCGG
857	ATGTCTAAAGGTGAAGAATTATTC
860	ATGGATGCAGAATTCCGACATG

Table S2. Oligonucleotides used in this study.